

A Neurogeometric Stereo Model for Individuation of 3D Perceptual Units

Maria Virginia Bolelli^{1,2,4(⋈)}, Giovanna Citti^{1,2}, Alessandro Sarti^{1,2}, and Steven Zucker³

- Department of mathematics, University of Bologna, Bologna, Italy giovanna.citti@unibo.it
 - ² Laboratoire CAMS, CNRS-EHESS, Paris, France alessandro.sarti@ehess.fr
- 3 Departments of Computer Science and Biomedical Engineering, Yale University, New Haven, CT, USA

steven.zucker@yale.edu

⁴ Laboratoire des Signaux et Systèmes, Université Paris-Saclay, CentraleSupèlec, Gif-sur-Yvette, France

maria-virginia.bolelli@centralesupelec.fr

Abstract. We present a neurogeometric model for stereo vision and individuation of 3D perceptual units. We first model the space of position and orientation of 3D curves in the visual scene as a sub-Riemannian structure. Horizontal curves in this setting express good continuation principles in 3D. Starting from the equation of neural activity we apply harmonic analysis techniques in the sub-Riemannian structure to solve the correspondence problem and find 3D percepts.

Keywords: Neurogeometry · Stereo vision · 3D perceptual units · 3D good continuation

1 Introduction

We propose here a neurogeometrical model of stereo vision, in order to describe the ability of the visual system to infer the three-dimensionality of a visual scene from the pair of images projected respectively on the left and right retina.

The first differential models of the visual cortex, devoted to the description of monocular vision, have been proposed by Hoffmann [16] and Koenderink-van Doorn [19]. Results were unified under the name of neurogeometry by Petitot and Tondut [23], who related psychophysical experiments of Field, Hayes and Hess [14] with the contact geometry introduced by Hoffmann [16] and the stochastic approach of Mumford [21]. The functional architecture of the visual cortex has been described through sub-Riemannian metrics by Citti and Sarti [8] and through Frenet frames by Zucker [29], and after that a large litterature was developed.

The geometric optics of stereo vision has been proposed by Faugeras in [13] and a differential model for stereo was proposed by Zucker [29]. A sub-Riemannian structure of 3D space has been introduced by Duits et al. in [11,12]

[©] The Author(s), under exclusive license to Springer Nature Switzerland AG 2023 F. Nielsen and F. Barbaresco (Eds.): GSI 2023, LNCS 14071, pp. 53–62, 2023. https://doi.org/10.1007/978-3-031-38271-0_6

and [24] for 3D image processing. Our model, first introduced in [4], generalizes these models introducing a sub-Riemannian geometry for stereo vision: it is presented in Sect. 3. In particular, we will focus on association fields, introduced in 2D by Field, Hayes and Hess in [14] and modeled in [8,23] and [5]. We will extend this approach to neural connectivity with integral curves and justify psychophysical experiments on perceptual organization of oriented elements in \mathbb{R}^3 ([9,15,17]).

The main contribution with respect to [4] is the constitution of 3D percepts, presented in Sect. 4. We start from the model of interactions between neural populations proposed by Bressloff-Cowan ([6]) and we modify the integro-differential equation they propose with the connectivity kernel obtained as fundamental solution of a sub-Riemannian Fokker Planck. Then, we generalize the stability analysis proposed by [6] for hallucinations, by [26] for emergence of percepts, and we show that in this case they correspond to 3D perceptual units.

2 The Stereo Problem

The stereo problem deals with the reconstruction of the three-dimensional visual scene starting from its perspective projection through left C_L and right C_R optical centers on the two eyes. The setting of the problem involves classical triangulation instruments (e.g. [13]), and the main issue is to couple in a correct way the correspondent left $Q_L = (x_L, y)$ and right $Q_R = (x_R, y)$ points on the parallel retinal planes $(y = y_L = y_R)$, in order to project them back into the environment space to obtain $Q = (r_1, r_2, r_3) \in \mathbb{R}^3$, see Fig. 1,(a). This goes under the name of stereo correspondence.

The main clues for solving the correspondence are the slight differences in the two projected images, namely the disparities. Our main focus will be on horizontal positional disparity $d := (x_L - x_R)/2$, which introduces the set of cyclopean coordinates (x, y, d), together with the mean position $x := (x_L + x_R)/2$. Since binocularly driven neurons in the primary visual cortex, which perform the binocular integration, receive input from monocular (orientation selective) cells, we will choose as additional variables the orientations on left and right monocular structures: θ_L and θ_R ; but we will not consider orientation disparity, because it does not seem to be coded directly in the visual cortex, see for example [7].

2.1 The Monocular Model for Orientation-Selective Cells

The hypercolumnar structure selective for orientation of monocular left and right simple cells in V1 (denoted respectively i = L, R) can be modeled in term of a fiber bundle, with base $(x_i, y) \in \mathbb{R}^2$ identified with the retinal plane, (see [23]) and fiber $\theta_i \in \mathbb{R}/2\pi\mathbb{Z} \equiv \mathbb{S}^1$. The response $O_i(x_i, y, \theta_i)$ of these cells to a visual signal on the retina $I(x_i, y)$ is quantified in terms of a function $\varphi(x_i, y, \theta_i)$, called receptive profile RP and well described by Gabor filters, see Fig. 1,(b). Following the work of Citti and Sarti [8], the action of these RPs induces a choice of contact

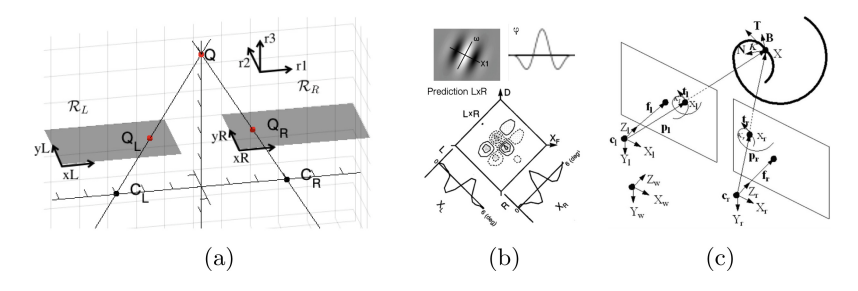


Fig. 1. (a) Stereo geometry. (b) Above: Gabor filter: model of 2D receptive profile, its 1D section. Below: binocular receptive profile (image adapted from [2]) (c) The Zucker model (image adapted from [20]).

form on the whole space:

$$\omega_{\theta_i} = -\sin\theta_i dx_i + \cos\theta_i dy. \tag{1}$$

The visual signal propagates in this cortical structure along integral curves of vector fields lying in the kernel of this contact form.

2.2 Models of Binocular Cells and Stereo Vision

Ohzawa et al. in [2] found that binocular simple cells in V1 perform a non-linear integration of left and right monocular cells, displayed in Fig. 1, (b). They proposed the binocular energy model (BEM), which characterize the binocular output through an interaction term O_B , product of left O_L and right O_R monocular outputs:

$$O_B = O_R O_L. (2)$$

The mathematical model for stereo vision built by Zucker et al. in [1,20] is based on neural mechanisms of selectivity to position, orientations and curvatures of the visual stimulus and it is expressed via instruments of Frenet differential geometry. The connections between binocular neurons are described by helices whose spiral develops along the depth axis, encoding simultaneously position and orientation disparities. The model is illustrated in Fig. 1, (c).

3 A Sub-Riemannian Model for Stereo Vision

In this section we present the biologically-inspired model proposed in [4].

3.1 The Fiber Bundle of Binocular Cells

The binocular structure is based on monocular ones and it is equipped with a symmetry that involves the left and right structures, allowing the use of cyclopean coordinates (x, y, d) defined in Sect. 2. The set of binocular cells will be

expressed a fiber bundle with base $\mathcal{B} = \mathbb{R}^2$ the cyclopean retina of coordinates (x,y). The structure of the fiber is $\mathcal{F} = \mathbb{R} \times \mathbb{S}^1 \times \mathbb{S}^1$, with coordinates $(d,\theta_L,\theta_R) \in \mathcal{F}$. Schematic representation is provided in Fig. 2, (a) and (b).

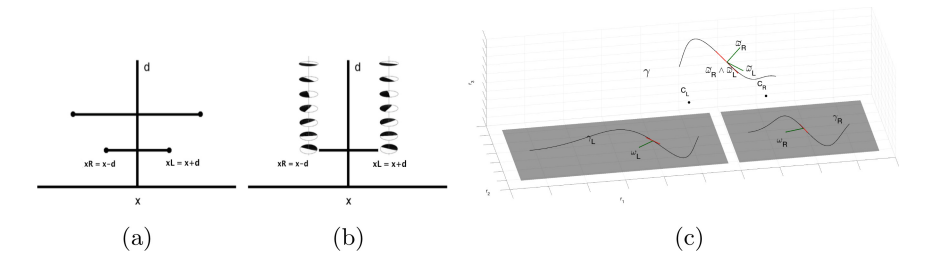


Fig. 2. Binocular cell structure and 3D reconstruction. (a) and (b) schematically represent the binocular fiber bundle in 2D: we visualized a 1D restriction to the direction x of the basis, the fiber of disparity d in (a) and the fiber of orientations θ_L and θ_R in (b). (c) describes reconstruction of a 3D curve from its projections. The normal to the curves γ_L and γ_R on retinal planes are identified by the 1-forms ω_{θ_L} and ω_{θ_R} . The wedge product $\tilde{\omega}_{\theta_L} \wedge \tilde{\omega}_{\theta_R}$ of their 3D counterpart identify the tangent vector to the 3D corresponding curve $\gamma : \mathbb{R} \to \mathbb{R}^3$.

3.2 Compatibility with Stereo Triangulation

We can introduce a 2-form starting from the monocular structures that embodies the binocular energy model, since Eq. (2) can be written in terms of monocular left and right RPs, see [4, Eq. (18),(49)], obtaining the following result.

Proposition 1. The binocular interaction term O_B of (2) can be recast as wedge product of the two monocular 1-forms ω_{θ_L} and ω_{θ_R} defined in (1):

$$O_B = \omega_{\theta_R} \wedge \omega_{\theta_L}. \tag{3}$$

It is possible to extend the monocular 1-forms ω_{θ_L} and ω_{θ_R} on retinal planes to $\tilde{\omega}_{\theta_L}$ and $\tilde{\omega}_{\theta_R}$ 1-forms in \mathbb{R}^3 and obtaining $\tilde{\omega}_{\theta_R} \wedge \tilde{\omega}_{\theta_L}$. Through the Hodge duality this 2-form identifies a vector that can be interpreted as the direction of the tangent to a potential 3D curve in the scene, see Fig. 2 (c).

So, binocular cells couple positions, identified with points in \mathbb{R}^3 , and orientations in \mathbb{S}^2 , identified with three-dimensional unitary tangent vectors. To solve the stereo problem the visual system must take into account suitable types of connections ([27]). It is therefore natural to introduce the perceptual space via the manifold $\mathcal{M} = \mathbb{R}^3_{(r_1, r_2, r_3)} \rtimes \mathbb{S}^2_{(\theta, \varphi)}$, and look for appropriate curves in \mathcal{M} .

3.3 Stereo Sub-Riemannian Geometry

The sub-Riemannian structure on \mathcal{M} can be expressed locally using the chart $\theta \in (0, 2\pi), \varphi \in (0, \pi)$ by considering an orthonormal frame $\{Y_3, Y_{\theta}, Y_{\varphi}\}$, where:

$$Y_3 = \cos\theta \sin\varphi \partial_1 + \sin\theta \sin\varphi \partial_2 + \cos\varphi \partial_3, \quad Y_\theta = \frac{1}{\sin\varphi} \partial_\theta, \quad Y_\varphi = \partial_\varphi. \tag{4}$$

The vector field Y_3 encodes the tangent of the stimulus, Y_{φ} involves orientation in the depth direction, while Y_{θ} involves orientation on the fronto-parallel plane. We take here into account that contour detectability systematically changed with the degree to which they are oriented in depth, see [18]. Indeed the vector Y_{θ} is not defined for $\varphi = 0$, meaning that we do not perceive correctly contours which are completely oriented in the depth direction. The vector fields satisfy the Hörmander condition since the whole space is spanned at every point by the vectors $\{Y_3, Y_{\theta}, Y_{\varphi}\}$ and their commutators.

Remark 1. As noted by Duits and Franken in [12], the space $\mathbb{R}^3 \rtimes \mathbb{S}^2$ can be identified with the quotient $SE(3)/\{0_{|\mathbb{R}^3}\} \times SO(2)$. Different sections have different invariance properties; in [24], the authors provide a section which preserves isotropy in the spherical tangent plane and give the same role to all the angular variables [11, Thm.1 and Thm.4].

Integral curves with constant coefficients in the local orthonormal frame (4) are defined by the differential equation:

$$\dot{\Gamma}(t) = \vec{Y}_{3,\Gamma(t)} + c_1 \vec{Y}_{\theta,\Gamma(t)} + c_2 \vec{Y}_{\varphi,\Gamma(t)} \quad c_1, c_2 \in \mathbb{R}.$$
 (5)

These curves, displayed in Fig. 3 (a), can be thought of in terms of trajectories in \mathbb{R}^3 describing a movement in the Y_3 direction, and by varying the coefficients c_1 and c_2 in \mathbb{R} , they can twist and bend in all space directions. Formally, the amount of "twisting and bending" in space is measured by curvature k and torsion τ , which in this setting read as: $k = \sqrt{c_1^2 + c_2^2}$, and $\tau = -c_1 \cot \varphi$.

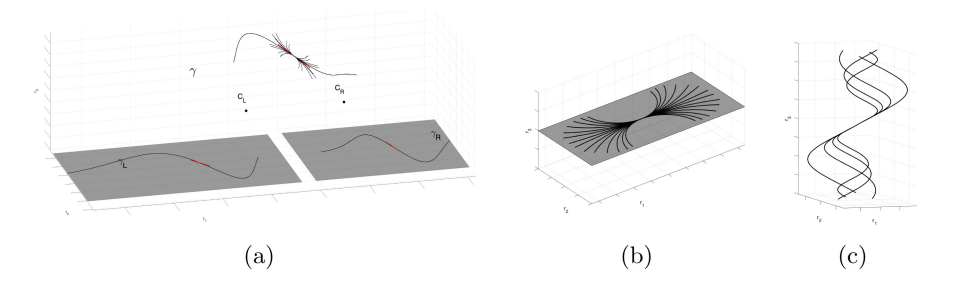


Fig. 3. Different families of integral curves (5). (a) General fan of integral curves described by Eq. (5) with varying c_1 and c_2 in \mathbb{R} , enveloping a curve $\gamma \in \mathbb{R}^3$. (b) Arc of circles for constant $\varphi = \pi/2$. (c) r3-helices for constant $\varphi = \pi/3$.

The model is then compatible with the previous models of [8] of monocular vision, since if $c_1 = 0$ or $\varphi = \pi/2$ then $\Gamma(t)_{|\mathbb{R}^3}$ is a piece of circle (Fig. 3, (b)). In addition it is compatible with the results of [1], based on properties of curvature, since if $\varphi = \varphi_0$ with $\varphi_0 \neq \pi/2$, then $\Gamma(t)_{|\mathbb{R}^3}$ is a r_3 -helix. The main difference is that curvature is an extracted feature in [1], while it is coded in connectivity in our model.

3.4 Good Continuation in 3D and Stereo Association Fields

The family (5) model neural connectivity (see [4]) and it can be related to the geometric relationships deriving from psychophysical experiments on perceptual organization of oriented elements in \mathbb{R}^3 , the basis of the Gestalt law of good continuation ([28]). This generalizes the 2D concept introduced by Field Hayes and Hess in [14] (Fig. 4, (a)) of an association field in 3D.

The geometrical affinities between orientations under which a pair of positionorientation elements in $\mathbb{R}^3 \times \mathbb{S}^2$ are perceived as connected in a 3D scene, have been determined by [17] with the theory of 3D relatability. Curves that are suitable to connect these 3D relatable points have the properties of being smooth and monotonic [9,15], extending good continuity/ regularity in depth. Moreover, the strength of the relatable edges in co-planar planes with the initial edge must meet the relations of the bi-dimensional association fields [17].

The family of integral curves (5) locally connects the association fan generated by 3D relatability geometry (Fig. 4, (b)), satisfying smoothness, monotonicity and compatibility with 2D association fields.

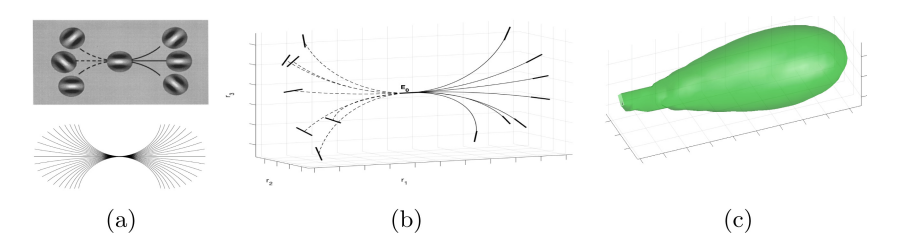


Fig. 4. Display of connectivity. (a) Field Hayes and Hess association field (top) and 2D integral curves of the Citti-Sarti model [8] (bottom). (b) Fan of 3D relatable points connected by integral curves (5).(c) Iso-surface in \mathbb{R}^3 of probability density (7) associated to the curves (5).

4 Constitution of 3D Visual Perceptual Units

Integral curves model the good continuation law, playing a fundamental role within the problem of perceptual grouping, individuating 3D visual units.

4.1 Sub-Riemannian Fokker Plank Equation and Connectivity Kernel

The emergence of 3D visual percepts derives from interactions between binocular cells: according to the Gestalt law of good continuation, entities described by similar local orientations are more likely to belong to the same perceptual unit.

Following [3,25], we suppose that the signal starting from a binocular neuron $\xi \in \mathbb{R}^3 \rtimes \mathbb{S}^2$ evolves following the stochastic process described by the SDE:

$$d\Gamma(t) = Y_{\mathbb{R}^3, \Gamma(t)} dt + \lambda(Y_{\theta, \Gamma(t)}, Y_{\varphi, \Gamma(t)}) dB(t), \quad \lambda \in \mathbb{R},$$
(6)

with B(t) 2-dimensional Brownian motion. The probability of interaction between points ξ and $\xi' \in \mathcal{M}$, has a (time-independent) density:

$$\{J_{\lambda}(\xi, \xi')\}_{\lambda \in \mathbb{R}},$$
 (7)

whose iso-surfaces in \mathbb{R}^3 are displayed in Fig. 4, (c). This probability density coincides with the (time-integrated) fundamental solution of the forward Kolmogorov differential equation associated to (6) with operator $\mathcal{L} = -Y_3 + \lambda (Y_\theta^2 + Y_\varphi^2)$ written in terms of the chosen vector fields (4). Analytical approximation of the fundamental solutions have been provided in [12,24], and numerical approximation with Fourier methods and Monte-Carlo simulations in [10]. We implement here the latter, following the approach presented in [3], since it is more physiological being based on the stochastic integral curves.

Remark 2. The authors in [24] have shown that the space $\mathbb{R}^3 \rtimes \mathbb{S}^2$ can be identified with a section of SE(3) where kernels have symmetry properties with respect to the group law, and all angles have the same role. In our model, 3D association field fan depends on the choice of the vector fields, which is not invariant, due to the different meaning of the considered orientations. Nevertheless, we expect the kernel to preserve invariance. A comparison between the two approaches based on parametrix method will be provided in a future paper.

4.2 From Neural Activity to 3D Perceptual Units

The kernels (7) are implemented as facilitation patterns to define the evolution in time $t \mapsto a(\xi, t)$ of the activity of the neural population at $\xi \in \mathcal{M}$. This activity is usually modeled through a mean field equation, see [6]:

$$\partial_t a(\xi, t) = -a(\xi, t) + \sigma \left(\int_{\mathcal{M}} J(\xi, \xi') a(\xi', t) d\xi' + h(\xi, t) \right), \tag{8}$$

where h is the feedforward input, σ is a sigmoidal function and J a symmetrization of (7). When the input h is constant over a subset Ω of \mathcal{M} and zero elsewhere, it has been proved in [26] that the domain of Eq. (8) reduces to Ω since the population activity is negligible in the complementary set $\mathcal{M} \setminus \Omega$.

We extend the stability analysis around a stationary state a_1 proposed by [6] for hallucination and [26] for perceptual units. A perturbation u, difference between two solutions $a - a_1$, satisfies the eigenvalue problem associated to the linearized time independent operator

$$\int_{\Omega} J(\xi, \xi') u(\xi', t) d\xi' = \frac{1}{\mu} u(\xi, t) \tag{9}$$

where $\mu = \sigma'(0)$. As shown in [26] for the 2D case, the eigenvectors represent the perceptual units, and the eigenvalues their salience. The whole process is strictly linked with spectral clustering and dimensionality reduction results ([22]).

4.3 The Proposed Model for the Correspondence Problem

The model can be described as follows. We start from two rectified stereo images. We couple all possible corresponding points (left and right retinal points with the same abscissa coordinate): this lifts retinal points in points $\xi_i \in \Omega$ generating also false matches, i.e. points that do not belong to the original stimulus. We call affinity matrix the kernel J evaluated on every couple of lifted points $\xi_i, \xi_j \in \Omega$: $\mathbf{J}_{i,j} := J(\xi_i, \xi_j)$. Spectral analysis on \mathbf{J} individuates 3D perceptual units, and solves the stereo correspondence. In this process false matches are eliminated since the similarity measure introduced by the kernel \mathbf{J} groups elements satisfying the good-continuation constraints.

4.4 Numerical Experiments

We develop the ideas illustrated so far by numerical examples; the main steps of the algorithm are summarized in Table 1.

Table 1. Recovering 3D visual percepts starting from rectified stereo images.

- Gabor filtering the left and right retinal images to obtain for every point (x_i, y_i) its corresponding orientation θ_i for i = L, R
- Recover the domain $\Omega \subset \mathbb{R}^3 \times \mathbb{S}^2$, $\xi_k \in \Omega, k = 1, \dots, n$, from the coupling of retinal images by inverting perspective projections.
- 2 Call affinity matrix **J** the discretization of the kernel $J: \mathbf{J}_{ij} := J(\xi_i, \xi_j)$.
- 3 Solve the eigenvalue problem $\mathbf{J}a = \iota a$.
- 4 Find the q largest eigenvalues $\{\iota_i\}_{i=1}^q$ and the associated eigenvectors $\{a_i\}_{i=1}^q$.
- 5 | For k = 1, ..., n assign the point ξ_k to the clustered labeled by $\max_i \{a_i(k)\}_{i=1}^q$.
- 6 Join together the clusters with less than Q elements.

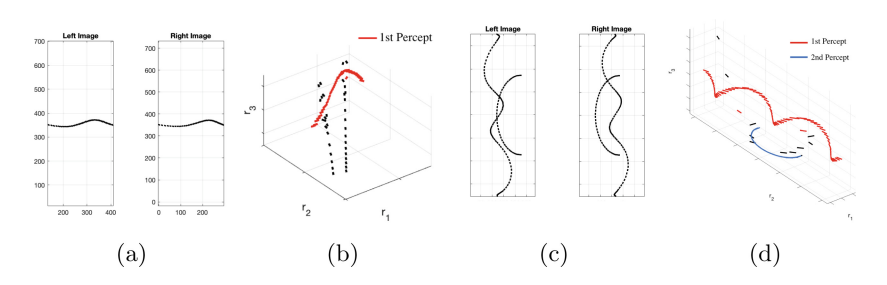


Fig. 5. (a) Stereo images of a 3D curve. (b) Lifting of the stimulus in $\mathbb{R}^3 \times \mathbb{S}^2$: points clustered together are marked by the same color (one main red colored 3D percept); black points do not belong to any cluster. (c) Stereo images of a 3D helix and arc of a circle. (d) Lifting of (c) in $\mathbb{R}^3 \times \mathbb{S}^2$: two main clusters (red and blue) correctly segment into two perceptual units the 3D visual scene. (Color figure online)

The model is first tested on synthetic stereo images of 3D curves (Fig. 5 (a),(c)), and perceptual units are correctly recovered (Fig. 5 (c),(d)).

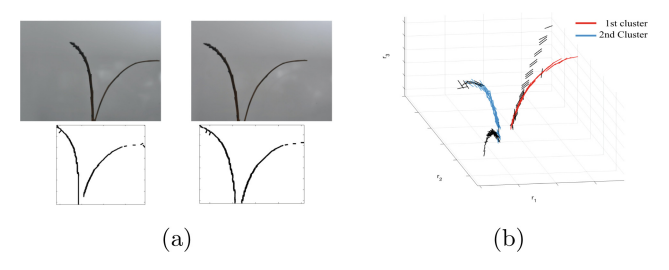


Fig. 6. (a) Top: couple of natural images. Bottom: Gabor filtering to recover position and orientation in retinal planes. (b) The application of the algorithm defined in Table 1 individuates the two 3D perceptual units (red and blue points). (Color figure online)

A second test is performed on a natural image: we pre-process the images via Gabor filtering, to recover position and orientation on the two retinas, and then we apply the model. Results are illustrated in Fig. 6.

Acknowledgement. MVB, GC, AS were supported by GHAIA project, H2020 MSCA RISE n. 777622 and by NGEU-MUR-NRRP, project MNESYS (PE0000006) (DN. 1553 11.10.2022). SWZ was supported by NIH Grant EY031059 and NSF CRCNS Grant 1822598.

References

- Alibhai, S., Zucker, S.W.: Contour-based correspondence for stereo. In: Vernon, D. (ed.) ECCV 2000. LNCS, vol. 1842, pp. 314–330. Springer, Heidelberg (2000). https://doi.org/10.1007/3-540-45054-8 21
- Anzai, A., Ohzawa, I., Freeman, R.: Neural mechanisms for processing binocular information i. simple cells. J. Neurophysiol. 82(2), 891–908 (1999)
- Barbieri, D., Citti, G., Cocci, G., Sarti, A.: A cortical-inspired geometry for contour perception and motion integration. J. Math. Imaging Vis. 49(3), 511–529 (2014)
- Bolelli, M.V., Citti, G., Sarti, A., Zucker, S.W.: Good continuation in 3D: the neurogeometry of stereo vision. arXiv preprint arXiv:2301.04542 (2023)
- Boscain, U., Duits, R., Rossi, F., Sachkov, Y.: Curve cuspless reconstruction via sub-riemannian geometry. ESAIM: Control, Optimisat, Calculus Variations 20, 748–770 (2014)
- Bressloff, P.C., Cowan, J.D.: The functional geometry of local and horizontal connections in a model of V1. J. Physiol. Paris 97(2), 221–236 (2003)
- Bridge, H., Cumming, B.: Responses of macaque V1 neurons to binocular orientation differences. J. Neurosci. 21(18), 7293-7302 (2001)
- 8. Citti, G., Sarti, A.: A cortical based model of perceptual completion in the roto-translation space. J. Math. Imaging Vis. **24**(3), 307–326 (2006)
- Deas, L.M., Wilcox, L.M.: Perceptual grouping via binocular disparity: The impact of stereoscopic good continuation. J. Vis. 15(11), 11 (2015)
- Duits, R., Bekkers, E.J., Mashtakov, A.: Fourier transform on the homogeneous space of 3D positions and orientations for exact solutions to linear pdes. Entropy 21(1), 38 (2019)
- Duits, R., Dela Haije, T., Creusen, E., Ghosh, A.: Morphological and linear scale spaces for fiber enhancement in dw-mri. J. Mathematical Imaging Vis. 46, 326–368 (2013)

- Duits, R., Franken, E.: Left-invariant diffusions on the space of positions and orientations and their application to crossing-preserving smoothing of HARDI images. IJCV (2011)
- Faugeras, O.: Three-dimensional computer vision: a geometric viewpoint. MIT press (1993)
- 14. Field, D.J., Hayes, A., Hess, R.F.: Contour integration by the human visual system: Evidence for a local "association field." Vision Res. **33**(2), 173–193 (1993)
- Hess, R.F., Hayes, A., Kingdom, F.A.A.: Integrating contours within and through depth. Vision. Res. 37(6), 691–696 (1997)
- Hoffman, W.C.: The visual cortex is a contact bundle. Appl. Math. Comput. 32(2), 137–167 (1989)
- Kellman, P.J., Garrigan, P., Shipley, T.F., Yin, C., Machado, L.: 3-d interpolation in object perception: Evidence from an objective performance paradigm. J. Exp. Psychol. Hum. Percept. Perform. 31(3), 558–583 (2005)
- 18. Khuu, S.K., Honson, V., Kim, J.: The perception of three-dimensional contours and the effect of luminance polarity and color change on their detection. J. Vis. (2016)
- 19. Koenderink, J.J., van Doorn, A.J.: Representation of local geometry in the visual system. Biol. Cybern. **55**(6), 367–375 (1987)
- Li, G., Zucker, S.W.: Contextual inference in contour-based stereo correspondence.
 IJCV 69(1), 59–75 (2006)
- Mumford, D.: Elastica and computer vision. In: Algebraic geometry and its applications, pp. 491–506. Springer (1994). https://doi.org/10.1007/978-1-4612-2628-4 31
- Perona, P., Freeman, W.: A factorization approach to grouping. In: Burkhardt, H., Neumann, B. (eds.) ECCV 1998. LNCS, vol. 1406, pp. 655–670. Springer, Heidelberg (1998). https://doi.org/10.1007/BFb0055696
- Petitot, J., Tondut, Y.: Vers une neurogéométrie. Fibrations corticales, structures de contact et contours subjectifs modaux. Math. Scien. Humain. 145, 5–101 (1999)
- 24. Portegies, J.M., Duits, R.: New exact and numerical solutions of the (convection-)diffusion kernels on SE(3). Differential Geom. Appl. **53**, 182–219 (2017)
- 25. Sanguinetti, G., Citti, G., Sarti, A.: A model of natural image edge co-occurrence in the rototranslation group. J. Vis. (2010)
- 26. Sarti, A., Citti, G.: The constitution of visual perceptual units in the functional architecture of V1. J. Comput. Neurosci. (2015)
- Scholl, B., Tepohl, C., Ryan, M.A., Thomas, C.I., Kamasawa, N., Fitzpatrick, D.: A binocular synaptic network supports interocular response alignment in visual cortical neurons. Neuron 110(9), 1573–1584 (2022)
- Wagemans, J., et al.: A century of gestalt psychology in visual perception: I perceptual grouping and figure-ground organization. Psych. Bull. 138(6), 1172 (2012)
- 29. Zucker, S.W.: Differential geometry from the Frenet point of view: boundary detection, stereo, texture and color. In: Handbook of Mathematical Models in Computer Vision, pp. 357–373. Springer (2006). https://doi.org/10.1007/0-387-28831-7 22